INTERNATIONAL JOURNAL OF
NUMERICAL ANALYSIS AND MODELING
Volume 10, Number 3, Pages 588–602

ON LINEAR FINITE ELEMENTS FOR SIMULTANEOUSLY RECOVERING SOURCE LOCATION AND INTENSITY

XIAOMAO DENG, YUBO ZHAO AND JUN ZOU

Abstract. Linear elements are least expensive finite elements for simultaneously recovering the source location and intensity in a general convection-diffusion process. However, the derivatives of the least-squares objective functional with Tikhonov regularizations are not well-defined when linear finite elements are used. In this work we provide a systematic formulation of the numerical inversion using linear finite elements and propose some effective techniques to overcome the undefinedness that may occur in inversion process. We show that linear finite elements can be made very robust and efficient in simultaneously recovering the source location and intensity. Numerical results are presented to validate the robustness and effectiveness of the proposed algorithm.

Key words. source location, source intensity, convection-diffusion and linear finite elements.

1. Introduction

Source isolation is an effective measure taken in practical applications for pollution prevention in groundwater, lakes and rivers, and for quick response to fire accidents or some attacks caused by airborne/aerosolized chemical or biological agent. The knowledge of the contaminant sources and their intensities plays an essential role in taking the measures. When the source location and intensity are available, one may simulate the distribution of the pollutant concentration and its transport process in the concerned environmental systems by a transport or convection-diffusion model [1, 11, 10, 15]. This is the so-called forward problem. But in many applications such as those aforementioned ones, the source location and intensity are the essential information one needs to make further actions. This can be achieved usually by solving an inverse transport or convection-diffusion problem, using some extra data of concentration or its fluxes measured by appropriately located sensors within a certain period of time. This inversion process may help recover the location, intensity or time release history of the pollutant sources. As a typical inverse problem the identification of the source location and intensity is severely ill-posed in the sense of Hadamard [5, 18, 19], that is, one of the three fundamental properties such as the existence, uniqueness and stability of solutions to the considered problem is not satisfied. For numerical processes, the most important property is the stability. The inverse problem of recovering the source location and intensity is typically unstable, i.e., small noise in the observation data may cause tremendous change of the source location and intensity.

Various approaches have been applied to the inverse problem of recovering the source intensity distribution [16, 17, 20] when the source location is known, or of recovering both the source intensity and location [1, 6, 7, 8, 11]. Quasi-explicit reconstruction formulae may exist for point source location recovery in one-dimensional cases under some careful design of the observation locations [7, 8], and the point source locations may be found by solving some integral equation involving the

Received by the editors July 1, 2012 and, in revised form, September 10, 2012.
2000 *Mathematics Subject Classification.* 35R35, 49J40, 60G40.

fundamental solutions in two dimensions for a heat conduction problem [9]. Regarding to the source intensity recovery, explicit formula is available for inversion in one-dimensional cases with constant coefficients and steady sources [11]. The method of quasi-reversibility was studied in [17] to retrace the plume history for one-dimensional cases, and a fourth-order term was added to the model to stabilize the numerical dispersion and counteract the data noise.

Optimization approaches are popular in solving various inverse problems [3, 13, 14, 21]. Linear programming and multiple regression method were applied in [6] for finding the pollutant source location and their magnitude in a simple one-dimensional model. When the source location is known, some numerical efforts were made to recover the time intensity of the source, e.g., in [16] for one dimension and in [20] for two dimensions. The Tikhonov regularization approach was used in [16], while an iterative method was applied in [20] without any regularization, so it works only for noise-free observation data, and performs poorly whenever there is noise present in the data.

In this work we will apply the popular output least-squares formulation with appropriate regularizations for simultaneously recovering the point source location and the corresponding time-dependent intensity profile. Our major investigation will be on the space discretization of the resulting nonlinear optimization system by the least expensive finite element method, namely the piecewise linear finite elements. There are two major reasons why we are interested in the use of linear elements. First, higher order finite elements are much more expensive than linear elements, especially in three-dimensions. Second, unlike for direct problems, higher order continuous finite elements do not bear any advantages over the linear elements for solving inverse problems. This is due to the fact that the solution of an inverse problem usually requires solving an adjoint problem corresponding to the forward model equation, but the regularity of the solution to the adjoint problem is usually low, often lower than H^2, no matter whether the domains or the coefficients involved in the concerned equations are smooth or not since the measurement data always serve as a source term of the adjoint problem and the data always contain noise in applications. Therefore high-order elements can not generate better accuracy than linear elements for inverse problems. The above two reasons show that linear elements are more practical and reasonable in terms of both accuracy and computational efficiency. This motivates our current investigation of linear elements for the inverse problem of simultaneously recovering the source location and its corresponding intensity. To the best of our knowledge, this practically important topic has not been studied in the literature. A major difficulty arises from the space singular delta function in the source term of the convection-diffusion model and the time singular delta function in the adjoint system. As we shall see, for the reconstruction of the source location we need to evaluate the derivatives of functions from the finite element space used, but that are unfortunately not well-defined along element edges (2D) or faces (3D) for piecewise linear finite elements. This difficulty can be naturally avoided by using higher order C^1 finite elements [4], but with much higher computational efforts, since many more degrees of freedom will be involved than the ones for linear elements. We shall propose two techniques to overcome such difficulty and show that linear finite elements can be made very robust and effective in simultaneously recovering the source location and intensity. So this work provides a complete formulation of the numerical inversion process using the linear finite elements.

The rest of the paper is arranged as follows. Section 2 introduces the model formulation; sections 3 and 4 discuss the mathematical formulation of the inverse problem and many technical issues involved in inversion using linear finite elements. Numerical experiments for the recovery of different source locations, smooth and discontinuous source intensity functions are given in section 5, and some concluding remarks are mentioned in section 6.

2. Model formulation

We consider a physical domain Ω where a heat or pollution source is present but its location $\mathbf{x}^*$ is unknown, and write the distribution of the temperature or pollutant concentration as $C(\mathbf{x}, t)$ at location $\mathbf{x}$ and time t. The distribution process $C(\mathbf{x}, t)$ can be modeled often by the following typical convection-diffusion system [1, 11, 15, 10], with a singular point source at location $\mathbf{x}^*$:

$$\frac{\partial C}{\partial t} = \nabla \cdot (a(\mathbf{x})\nabla C) - \nabla \cdot (\mathbf{v}(\mathbf{x})C) + \delta(\mathbf{x} - \mathbf{x}^*)f(t), \quad 0 \le t \le T\,,\ \mathbf{x} \in \Omega \tag{1}$$

where $f(t)$ is the temporal intensity of the source at location $\mathbf{x}^*$, $a(\mathbf{x})$ and $\mathbf{v}(\mathbf{x})$ are the diffusivity and convection coefficient. We will complement the model by the following mixed boundary conditions

$$C(\mathbf{x}, t) = p(\mathbf{x}, t), \quad \mathbf{x} \in \Gamma_1\,; \quad a(\mathbf{x})\frac{\partial C}{\partial \mathbf{n}} = q(\mathbf{x}, t), \quad \mathbf{x} \in \Gamma_2 \tag{2}$$

and the initial condition

$$C(\mathbf{x}, 0) = C_0(\mathbf{x}), \quad \mathbf{x} \in \Omega\,, \tag{3}$$

where Γ_1 and Γ_2 are two separated parts forming the entire physical boundary $\partial\Omega$.

The main concern of this work is to study the inverse problem: Given the measurement data $C^\varepsilon(\mathbf{x})$ of the concentration $C(\mathbf{x}, t)$ at the terminal time T in Ω or at a set of specified locations $\mathbf{x}_1, \mathbf{x}_2, \cdots, \mathbf{x}_{N_s}$ inside Ω, recover the location $\mathbf{x}^*$ and time-dependent intensity $f(t)$ of the source in equation (1).

3. Mathematical formulation of the inverse problem

The inverse source problem of our interest is severely ill-posed. In order to handle the ill-posedness, we will take the Tikhonov regularization approach for the numerical reconstruction of the location $\mathbf{x}^*$ and intensity $f(t)$ of the source in equation (1). This converts our reconstruction process into a nonlinear optimization of the form

$$J(f, \mathbf{x}^*) = \frac{1}{2}\int_\Omega (C(\mathbf{x}, T) - C^\varepsilon(\mathbf{x}))^2\, d\mathbf{x} + \frac{\beta}{2}N(f), \tag{4}$$

when the measurement data $C^\varepsilon(\mathbf{x})$ is available over the whole domain Ω (possibly after interpolating some scattered data), or

$$J(f, \mathbf{x}^*) = \frac{1}{2}\sum_{i=1}^{N_s}(C(\mathbf{x}_i, T) - C^\varepsilon(\mathbf{x}_i))^2 + \frac{\beta}{2}N(f), \tag{5}$$

when the measurement data is available only partially, namely, at a set of specified locations $\mathbf{x}_1, \mathbf{x}_2, \cdots, \mathbf{x}_{N_s}$ in Ω. Concentration $C(\mathbf{x}, t)$ in (4) or (5) is the solution to the convection-diffusion system (1)-(3) associated with the location $\mathbf{x}^*$ and source intensity $f(t)$. The second term in (4) is the regularization term, where β is the regularization parameter and $N(f)$ is the regularization which may take different forms depending on our a priori information on the smoothness of the physical

source intensity $f(t)$. We shall consider the following three different forms, namely the L^2-, H^1- and BV-regularization:

$$N(f) = \int_0^T f(t)^2 dt\,, \quad N(f) = \int_0^T |f_t(t)|^2 dt\,, \quad N(f) = \int_0^T |Df|\,. \tag{6}$$

For the sake of convenience, we shall write (4) and (5) into a unified form

$$J(f, \mathbf{x}^*) = \frac{1}{2}\int_\Omega A(\mathbf{x})(C(\mathbf{x}, T) - C^\varepsilon(\mathbf{x}))^2\, d\mathbf{x} + \frac{\beta}{2}N(f), \tag{7}$$

where $A(\mathbf{x})$ is the data range indicator function, namely $A(\mathbf{x}) = 1$ corresponds to (4), and $A(\mathbf{x}) = \sum_{i=1}^{N_s} \delta(\mathbf{x} - \mathbf{x}_i)$ corresponds to (5). In some applications one individual form from (6) may not work well, then we may use the mixed regularizations. For instance, we may mix the first and third regularizations from (6), then we should replace the last term in (7) by

$$\frac{\beta_1}{2}\int_0^T f(t)^2 dt + \beta_2 \int_0^T |Df|\,. \tag{8}$$

4. Technical issues in optimization using linear finite elements

In this section we discuss some technical issues involved in minimizing the nonlinear objective functional (7) using linear finite elements, including discretization, gradient computing, adjoint systems, numerical challenges and their remedies.

Let $\mathcal{T}^h$ be a regular triangulation of Ω with triangular elements [4]. We define V^h to be the finite element space consisting of continuous piecewise linear functions on $\mathcal{T}^h$, and $\mathring{V}^h$ to be the subspace of V^h with functions vanishing on the Dirichlet boundary Γ_1. To fully discretize the system (7), we partition the time interval $[0, T]$ as $0 = t^0 < t^1 < \cdots < t^M = T$, with $t^n = n\tau, \tau = T/M$. For a given sequence $\{C^n\}$ and a function $C(\mathbf{x}, t)$, we define the difference quotient and the averaging function:

$$\partial_\tau C^n = \frac{C^n - C^{n-1}}{\tau}, \quad \bar{C}^n(\mathbf{x}) = \frac{1}{\tau}\int_{t^{n-1}}^{t^n} C(\mathbf{x}, t) dt\,.$$

Let π_h be the finite element interpolation associated with the space V^h, and C_h^n be the finite element approximation of $C(\mathbf{x}, t)$ at time t^n, then we can discretize the system (1)-(3) by the Crank-Nicolson scheme in time and piecewise linear finite elements in space as follows:

Find the sequence of approximations C_h^0, C_h^1, $\cdots$, C_h^M such that $C_h^0 = \pi_h C_0$, and $C_h^n \in V^h$ satisfying $C_h^n(\mathbf{x}) = \pi_h p(\mathbf{x}, t^n)$ for $\mathbf{x} \in \Gamma_1$ and

$$\begin{aligned}(\partial_\tau C_h^n, w_h) + (a\nabla \bar{C}_h^n, \nabla w_h) + (\nabla \cdot (\mathbf{v}\bar{C}_h^n), w_h) = \\ w_h(\mathbf{x}^*)\bar{f}^n + \langle \bar{q}^n, w_h\rangle_{\Gamma_2}\ \forall\, w_h \in \mathring{V}^h\end{aligned} \tag{9}$$

where (u, v) and $\langle u, v\rangle_{\Gamma_2}$ are used for the integral of the product of any two functions u and v over Ω and Γ_2 respectively. Recall that we look for the source location $\mathbf{x}^*$ and intensity $f(t)$ in our inverse problem, so we will often write the finite element solution C_h^n in (9) as $C_h^n(f^\tau, \mathbf{x}^*)$ to emphasize its dependence on f and $\mathbf{x}^*$, where $f^\tau(t)$ denotes the continuous piecewise linear function which takes the value $f^n = f(t^n)$ at the time t^n for $n = 0, 1, \cdots, M$.

Now using the sequence of finite element solutions C_h^n from (9), we propose to approximate the functional (7) by

$$J_h^\tau(f^\tau, \mathbf{x}^*) = \frac{1}{2}\int_\Omega A(\mathbf{x})(C_h^M(f^\tau, \mathbf{x}^*) - C^\varepsilon)^2(\mathbf{x})\, d\mathbf{x} + \frac{\beta}{2}N(f^\tau)\,. \tag{10}$$

4.1. Gradients of the objective functional. One can apply any existing iterative optimization algorithm to minimize the nonlinear functional (10), e.g., the steepest descent and nonlinear conjugate gradient method. A key ingredient in realizing these methods is to determine the search direction in each iteration, for which we need to evaluate the gradient of functional J_h^τ in (10) with respect to the unknown source location $\mathbf{x}^*$ and intensity f^τ.

Next we take the L^2 regularization, i.e., the first form in (6), as an example to illustrate the evaluation of the gradient of J_h^τ. Using the definition (10), we can easily write the derivative of J_h^τ with respect to intensity f^τ in direction g^τ, the derivatives of J_h^τ with respect to the coordinates of $\mathbf{x}^*$ as follows:

$$(11)\quad (J_h^\tau)'(f^\tau,\mathbf{x}^*)g^\tau = \int_\Omega A(\mathbf{x})(C_h^M(f^\tau,\mathbf{x}^*)-C^\varepsilon)(\mathbf{x})D_h^M(\mathbf{x})\,d\mathbf{x}+\beta(f^\tau,g^\tau)\,,$$

$$(12)\quad (J_h^\tau)_{x_1}(f^\tau,\mathbf{x}^*) = \int_\Omega A(\mathbf{x})(C_h^M(f^\tau,\mathbf{x}^*)-C^\varepsilon)(\mathbf{x})E_h^M(\mathbf{x})\,d\mathbf{x}\,,$$

$$(13)\quad (J_h^\tau)_{x_2}(f^\tau,\mathbf{x}^*) = \int_\Omega A(\mathbf{x})(C_h^M(f^\tau,\mathbf{x}^*)-C^\varepsilon)(\mathbf{x})F_h^M(\mathbf{x})\,d\mathbf{x}$$

where $D_h^n = C_h^n(f^\tau,\mathbf{x}^*)'g^\tau$ is the derivative of C_h^n at f^τ in direction g^τ, $E_h^n = (C_h^n)_{x_1}$ and $F_h^n = (C_h^n)_{x_2}$ are the derivatives of C_h^n with respect to the coordinates of $\mathbf{x}^*$. And we know from (9) that $D_h^0 = 0$, and $D_h^n \in \mathring{V}^h$ for $n = 1, 2, \cdots, M$ solves the finite element equation $\forall\, w_h \in \mathring{V}^h$

$$(14)\qquad (\partial_\tau D_h^n, w_h) + (a\nabla \bar{D}_h^n, \nabla w_h) + (\nabla\cdot(\mathbf{v}\bar{D}_h^n), w_h) = w_h(\mathbf{x}^*)\bar{g}^n$$

while $E_h^0 = F_h^0 = 0$ and $E_h^n, F_h^n \in \mathring{V}^h$ for $n = 1, 2, \cdots, M$ solve the equations $\forall\, w_h \in \mathring{V}^h$

$$(15)\qquad (\partial_\tau E_h^n, w_h) + (a\nabla \bar{E}_h^n, \nabla w_h) + (\nabla\cdot(\mathbf{v}\bar{E}_h^n), w_h) = (w_h)_{x_1}(\mathbf{x}^*)\bar{f}^n$$

$$(16)\qquad (\partial_\tau F_h^n, w_h) + (a\nabla \bar{F}_h^n, \nabla w_h) + (\nabla\cdot(\mathbf{v}\bar{F}_h^n), w_h) = (w_h)_{x_2}(\mathbf{x}^*)\bar{f}^n$$

4.2. Adjoint systems. One can easily see that it is very expensive to evaluate the derivative of J_h^τ with respect to the intensity f^τ using the formula (11) since it requires solving one finite element system (14) for every basis direction g^τ. To reduce the computational costs, we apply an adjoint technique. To do so, we first derive an appropriate adjoint system for the continuous functional $J(f,\mathbf{x}^*)$ in (7) associated with the system (1)-(3).

Let $W^{1,p}(\Omega)$ and $W^{1,q}(\Omega)$ be the standard Sobolev spaces with $p, q > 0$ satisfying $1/p + 1/q = 1$. We can formally write (1) as an operator equation $L(C, f) = 0$, then introduce a corresponding Lagrange multiplier $G \in W^{1,p}(\Omega)$ and the Lagrange functional:

$$(17)\quad \mathcal{J}(C,f,G) = \frac{1}{2}\int_\Omega A(\mathbf{x})(C(\mathbf{x},T)-C^\varepsilon(\mathbf{x}))^2 d\mathbf{x} + \frac{\beta}{2}\int_0^T f(t)^2 dt + \int_0^T (G, L(C,f))dt\,.$$

By taking the derivative of $\mathcal{J}$ in (17) with respect to C at an arbitrary direction $\hat{C}$, and using the integration by parts and the arbitrariness of $\hat{C}$, we can deduce the adjoint system for the Lagrange multiplier G, namely $G(\mathbf{x},T) = 0$ for $\mathbf{x} \in \Omega$, $G(\mathbf{x},t) = 0$ on Γ_1 and $G(\mathbf{x},t) \in W^{1,p}(\Omega)$ satisfies

$$\begin{aligned} & -(G_t, w) + (a\nabla G, \nabla w) - (\mathbf{v}\cdot\nabla G, w) + \langle \mathbf{v}\cdot\mathbf{n} G, w\rangle_{\Gamma_2} \\ (18)\qquad = \; & -(\delta(t-T)A\,(C(\cdot,t)-C^\varepsilon), w)\,. \end{aligned}$$

for all $w \in W^{1,q}(\Omega)$ such that $w = 0$ on Γ_1. Then using the adjoint system (18), we can write the derivative of $J(f, \mathbf{x}^*)$ in (7) as

$$J'(f, \mathbf{x}^*)g = \int_0^T (-G(\mathbf{x}^*, t) + \beta f(t))g(t)dt\,. \tag{19}$$

Now using the Crank-Nicolson scheme for time marching and piecewise linear finite element space $\mathring{V}^h$ for space discretization we can write the finite element approximation of (18) as follows: Find $G_h^n \in \mathring{V}^h$ $(0 \le n \le M)$ such that $G_h^M = 0$ and satisfies

$$\begin{aligned} &-(\partial_\tau G_h^n, w_h) + (a\nabla \bar{G}_h^n, \nabla w_h) - (\mathbf{v}\cdot\nabla \bar{G}_h^n, w_h) + \langle \mathbf{v}\cdot\mathbf{n}\bar{G}_h^n, w_h\rangle_{\Gamma_2} \\ &= -\delta_{nM}(A\,(C_h^n - C^\varepsilon), w_h) \quad \forall w_h \in \mathring{V}^h \end{aligned} \tag{20}$$

where $\delta_{nM} = 0$ for $n \neq M$, and $\delta_{MM} = \frac{1}{2}$. Using this discrete adjoint system (20), we can get the discrete counterpart of the derivative of $J(f, \mathbf{x}^*)$ in (19), that greatly simplifies the derivative in (11):

$$(J_h^\tau)'(f^\tau, \mathbf{x}^*)g^\tau = \int_0^T (-G_h^\tau(\mathbf{x}^*, t) + \beta f^\tau)g^\tau dt\,. \tag{21}$$

Remark 4.1. *Considering the fact that the source is specified at the terminal $t = T$ in the adjoint system (20), we can not apply the backward Euler scheme for time-marching as it can not access the data at the terminal T. This is why we have used the Crank-Nicholson scheme for time marching in (20).*

4.3. Optimization algorithm. With the gradient information of functional J_h^τ in (10), we may apply any existing iterative optimization algorithm to minimize the nonlinear functional J_h^τ. As an example, we now formulate an algorithm using the nonlinear conjugate gradient method to update the source intensity $f(t)$ and the steepest descent method to update the source location $\mathbf{x}^*$.

Reconstruction Algorithm I. Select the initial guesses $\mathbf{x}^0$, f^0, and set $k := 0$.

(1) Solve the adjoint system (20) for $\{G_h^n(\mathbf{x}^k, f^k)\}$;
Solve the equations (15) and (16) respectively for $\{E_h^n(\mathbf{x}^k, f^k)\}$ and $\{F_h^n(\mathbf{x}^k, f^k)\}$.
(2) Apply the nonlinear CG method to update f^k: $f^{k+1} = f^k + \alpha_1^k d^k$.
(3) Update $\mathbf{x}^k = (x_1^k, x_2^k)$:
$$x_1^{k+1} = x_1^k - \alpha_2^k (J_h^\tau)_{x_1}(f^{k+1}, \mathbf{x}^k), \quad x_2^{k+1} = x_2^k - \alpha_3^k (J_h^\tau)_{x_2}(f^{k+1}, \mathbf{x}^k).$$
(4) Stop the iteration if the stopping criteria are satisfied; otherwise set $k := k + 1$ and go to step 1.

Remark 4.2. *In this remark we explain how to update in our numerical experiments the search direction d_k and stepsizes α_1^k, α_2^k and α_3^k in Reconstruction Algorithm I. We use the Fletcher-Reeves (FR) formula to update the nonlinear CG direction d^k: $d^k = J_k' + \gamma_k d^{k-1}$, with $d^0 = J_0'$ and $\gamma_k = \|J_k'\|^2/\|J_{k-1}'\|^2$ and $J_k' = -(J_h^\tau)'(f^k, \mathbf{x}^k)$ being the negative gradient direction which is obtained from formula (21). We select the stepsize α_1^k such that $\alpha_1^k = argmin_{\gamma>0} J_h^\tau(f^k + \gamma d_k)$. For the L^2 and H^1 regularizations in (6), we can work out the exact formulae:*

$$\alpha_1^k = -\frac{(C_h^M(f^k, \mathbf{x}^k) - C^\varepsilon, A_h^M) + \beta(f^k, d^k)}{(A_h^M, A_h^M) + \beta(d^k, d^k)} \quad (L^2 \text{ regularization}),$$

$$\alpha_1^k = -\frac{(C_h^M(f^k, \mathbf{x}^k) - C^\varepsilon, A_h^M) + \beta(\nabla f^k, \nabla d^k)}{(A_h^M, A_h^M) + \beta(\nabla d^k, \nabla d^k)} \quad (H^1 \text{ regularization})$$

where $A_h^M = C_h^M(f^k, \mathbf{x}^k)'d^k$. *For the BV regularization, we solve the one-dimensional optimization approximately for the optimal stepsize* α_1^k *by applying the back-tracking rule, namely we start with* α_1^k *of the same order as* $\|f^k\|/\|d^k\|$, *then reduce* α_1^k *by half until the functional* J_h^τ *reduces, i.e.* $J_h^\tau(f^{k+1}, \mathbf{x}^k) < J_h^\tau(f^k, \mathbf{x}^k)$. *The stepsize* α_2^k *and* α_3^k *are also determined by applying the back-tracking rule, namely they start from some values of the same order as* $|x_1^k|/\|(J_h^\tau)_{\mathbf{x}}(\mathbf{x}^k)\|$ *and* $|x_2^k|/\|(J_h^\tau)_{\mathbf{x}}(\mathbf{x}^k)\|$ *respectively, then reduce both* α_2^k *and* α_3^k *by half until the functional* J_h^τ *satisfies* $J_h^\tau(f^{k+1}, \mathbf{x}^{k+1}) < J_h^\tau(f^{k+1}, \mathbf{x}^k)$.

4.4. Difficulties and remedies in evaluating derivatives of finite element functions. As it is directly observed from the right-hand sides of the equations (15) and (16), we need to evaluate the derivatives of piecewise linear functions from $\mathring{V}^h$ in order to compute the derivatives of the objective functional J_h^τ in (10) with respect to the coordinates of the unknown source location $\mathbf{x}^*$. Noting that these finite element functions from $\mathring{V}^h$ are continuous everywhere, but their derivatives are piecewise constant and defined only within each finite element, so have no meanings at element vertices as well as along all common edges shared by two neighboring elements. Therefore the derivatives of J_h^τ with respect to the coordinates of the source location $\mathbf{x}^*$ (see (12) and (13)) do not make sense when the approximate source location $\mathbf{x}^k$ happens to be at an element vertex or lies on some element edge during the iterations. A natural way to overcome such numerical difficulties is to use higher order C^1 elements [4], but these elements are too expensive, especially in three dimensions and for our current inverse problem, which is highly unstable and time-consuming itself. On the other hand, higher order C^1 elements do not provide any better accuracy than the piecewise linear C^0 elements for the entire inversion process as the highest regularity of the solution to the continuous adjoint system is at most H^2 due to the noisy data serving as the source term in the adjoint system; see (18).

In the rest of this section we shall propose several remedies to make it feasible for us to still use piecewise linear finite element spaces, that are continuous finite elements of lowest order, also the least expensive ones. This last fact serves as a very important ingredient to the final efficiency of our current entire numerical inversion process. One can easily observe from the equations (15)-(16) that the piecewise constant finite elements are infeasible to our current inverse problem since they generate only trivial solutions to (15)-(16). We shall demonstrate some effective treatments to evaluate the derivatives of piecewise linear finite element functions along all the common edges shared by two neighboring elements.

4.4.1. Averaging schemes. A simplest treatment to avoid the undefinedness of the derivatives of a piecewise linear finite element function w_h (see (15)-(16)) needed for computing the derivatives of functional J_h^τ in (10) with respect to the source location $\mathbf{x}^*$ is to take the derivatives of w_h at a given point $\mathbf{x}$ by using the corresponding derivatives of w_h in any one element where $\mathbf{x}$ is located. However, this treatment may produce unbalanced or poor results when the given point $\mathbf{x}$ is a common vertex shared by several neighboring elements or located on (or very closely to) the common edge of two neighboring elements. Indeed this is confirmed by many of our numerical simulations: the approximated source location point $\mathbf{x}^k$ gets frequently trapped in one element after the first few iterations.

A more effective treatment is to take the average of the derivatives of w_h at a given point $\mathbf{x}$ in those elements which share the point. The detailed procedure is as follows: when the iterative location $\mathbf{x}^k$ is inside an element T_i, then we simply take

the derivatives of w_h at this point; if $\mathbf{x}^k$ is located on some common edge shared by two elements or at some vertex shared by several elements, then the derivatives of w_h are computed by taking the average of its derivatives in those elements which share the point $\mathbf{x}^k$. This treatment takes care of the derivative information from all neighboring elements that share the approximate location point $\mathbf{x}^k$, thus it proves to work much better than the previous simplest technique, as we will see in the numerical experiments in Section 5.

4.4.2. Approximation of Dirac delta function. The averaging schemes proposed in section 4.4.1 work satisfactorily, but it requires to locate all the neighboring elements that share the approximate source point $\mathbf{x}^k$ during each iteration. We now present a more systematic treatment. This treatment is to reformulate the finite element equations (15)-(16) by approximating the singular delta functions by some smoother functions so that the derivatives of piecewise linear finite element functions w_h are needed only inside elements, not on any element edges any more.

Dirac delta function $\delta(x - x^*)$ can be regarded as the weak limit of a sequence of smooth functions $\{\delta_a\}$ with a spike at a given point x^*, namely

$$\lim_{a\to 0+} \int_{\mathbf{R}} \delta_a(x - x^*) f(x) = f(x^*),$$

for all compactly supported continuous function f. Many such approximations are available, such as the following Gaussian function δ_a^1, Lorentz-Cauchy function δ_a^2 and hyperbolic function δ_a^3 (see [2, 20]):

$$\begin{aligned}
\delta_a^1(x - x^*) &= \frac{1}{a\sqrt{\pi}} e^{-\frac{(x-x^*)^2}{a^2}}, \\
\delta_a^2(x - x^*) &= \frac{a/\pi}{a^2 + (x - x^*)^2}, \\
\delta_a^3(x - x^*) &= \frac{1}{2a\cosh^2(\frac{x-x^*}{a})}.
\end{aligned}$$

One can easily test numerically that the above three functions are nearly zero for almost all x except near $x = x^*$, where the values of these functions tend to infinity as $a \to 0$, and that their integrals over $[-l, l]$ is approaching to one as $a \to 0$ and $l \to \infty$.

With these approximate delta functions δ_a, we can now replace the equations (15) and (16) by the following two:

$$(\partial_\tau E_h^n, w_h) + (a\nabla \bar{E}_h^n, \nabla w_h) + (\nabla \cdot (\mathbf{v}\bar{E}_h^n), w_h) = ((w_h)_{x_1}, \delta_a(x_1 - x_1^*)\delta_a(x_2 - x_2^*))\bar{f}^n(t)$$
$$(\partial_\tau F_h^n, w_h) + (a\nabla \bar{F}_h^n, \nabla w_h) + (\nabla \cdot (\mathbf{v}\bar{F}_h^n), w_h) = ((w_h)_{x_2}, \delta_a(x_1 - x_1^*)\delta_a(x_2 - x_2^*))\bar{f}^n(t)$$

for any $w_h \in \mathring{V}^h$. We can see that the right-hand sides of these two equations are now well defined and can be computed elementwise, since the derivatives of w_h appear as part of the integrand, and the *undefined* pointwise evaluations of w_h are no longer needed, unlike in the original formulations (15) and (16). As we will see in the numerical experiments in Section 5, these treatments work very well.

5. Numerical Examples

We present in this section some numerical examples of recovering both the source location $\mathbf{x}^*$ and the intensity function $f(t)$ in the system (1). We set the testing domain to be $\Omega = (-2, 2) \times (-1, 1)$, and the terminal time at $T = 1$. Homogeneous Dirichlet and Neumann conditions are imposed on $\Gamma_1 = \{\mathbf{x} = (x_1, x_2);\ |x_1| = 2\}$ and $\Gamma_2 = \{\mathbf{x} = (x_1, x_2);\ |x_2| = 1\}$ respectively. Unless otherwise specified

the diffusion and convection coefficients $a(\mathbf{x})$ and $\mathbf{v}(\mathbf{x})$ are chosen to be 1.0 and $(1.0, 1.0)^T$ respectively. In order to generate the observation data, we first solve the forward convection-diffusion system (1)-(3) with a very fine mesh, 513×257, and the time stepsize $\tau = 1/100$, then add a random noise of the following form to the terminal concentration $C(\mathbf{x}, T)$:

$$C^{\varepsilon}(\mathbf{x}) = C(\mathbf{x}, T) + \varepsilon\, r\, C(\mathbf{x}, T),$$

where r is the uniform distribution function in $[-1, 1]$, and ε is the noise level. In our numerical experiments, we take the noise level to be $\varepsilon = 3\%$. In each example we will show both the true intensity function $f(t)$ and its reconstructed one f^k, as well as the convergence history of the approximate source location $\mathbf{x^k} = (x_1^k, x_2^k)$.

Example 1. We take the true intensity function and the source location to be

$$f(t) = t^2, \quad \mathbf{x}^* = (1.1, 0.1)$$

and their initial guesses to be

$$f^0(t) = 0.01, \quad \mathbf{x}^0 = (0.9, 0.3).$$

In our numerical inversion we take the mesh and the time step size to be 33×17 and $\tau = 1/50$ respectively. Figure 1 shows the numerical reconstructed source intensity $f(t)$ and the convergence history of the source location using the H^1 regularization with regularization parameter $\beta = 8.0e^{-6}$. One can see that the numerical reconstruction algorithm performs very well: it converges very stably and quickly for both the source location (12 iterations) and intensity function (36 iterations).

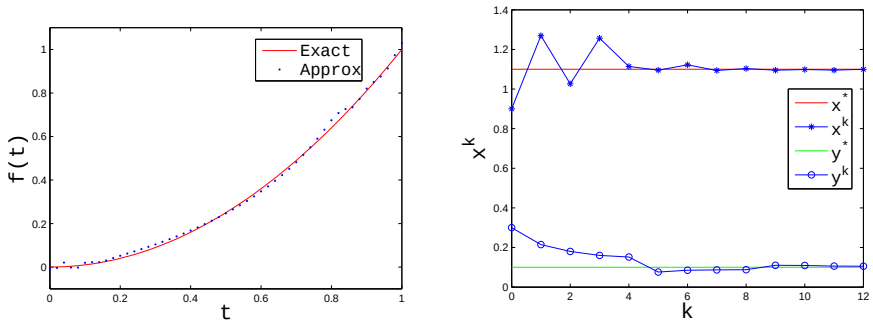

FIGURE 1. Reconstruction for Example 1

Remark 5.1. *We have also tried the steepest descent method for reconstructing the intensity function $f(t)$ and found that nonlinear CG method usually converges much faster. This is also true for the remaining Examples 2 and 3.*

Example 2. We take the true intensity function and source location to be

$$f(t) = \frac{75}{4} t(1-t)(\frac{1}{6} - t)^2 + 1.0, \quad \mathbf{x}^* = (-0.5, 0.5)$$

and their initial guesses to be

$$f^0 = 1.0 + 0.3t, \qquad \mathbf{x}^0 = (-0.2, 0.75).$$

In this example, we compare the reconstruction results for different amount of measurement data used, with a mesh 33×17 and time step size $\tau = 1/40$. Let

N_s be the number of locations where the data are collected, then we consider the following two cases:

(1) $N_s = 25$, data points $\{\mathbf{x}_{ij} = (-2+i, -1+0.5j), i, j = 0, 1, 2, 3, 4\}$;
(2) $N_s = 9$, data points $\{\mathbf{x}_{ij} = (-1+i, -0.5+0.5j), i, j = 0, 1, 2\}$.

We test a mixed L^2 and H^1 regularization, with two regularization parameters to be $\beta_1 = 10^{-2}$ and $\beta_2 = 10^{-3}$ for case 1 with $N_s = 25$, and $\beta_1 = 0$ and $\beta_2 = 7\times 10^{-5}$ for case 2 with $N_s = 9$. The reconstruction results are also given for a finer set of data points, $N_s = 33 \times 17 = 561$, with the regularization parameters $\beta_1 = 0$ and $\beta_2 = 5\times 10^{-5}$. From Figure 2 we observe that the reconstruction results deteriorate slowly as we can expect, but the convergence becomes slower and slower when we reduce the number of measured data points. However, as we observe, we can still obtain reasonable reconstruction even with as less as $N_s = 25$ data points.

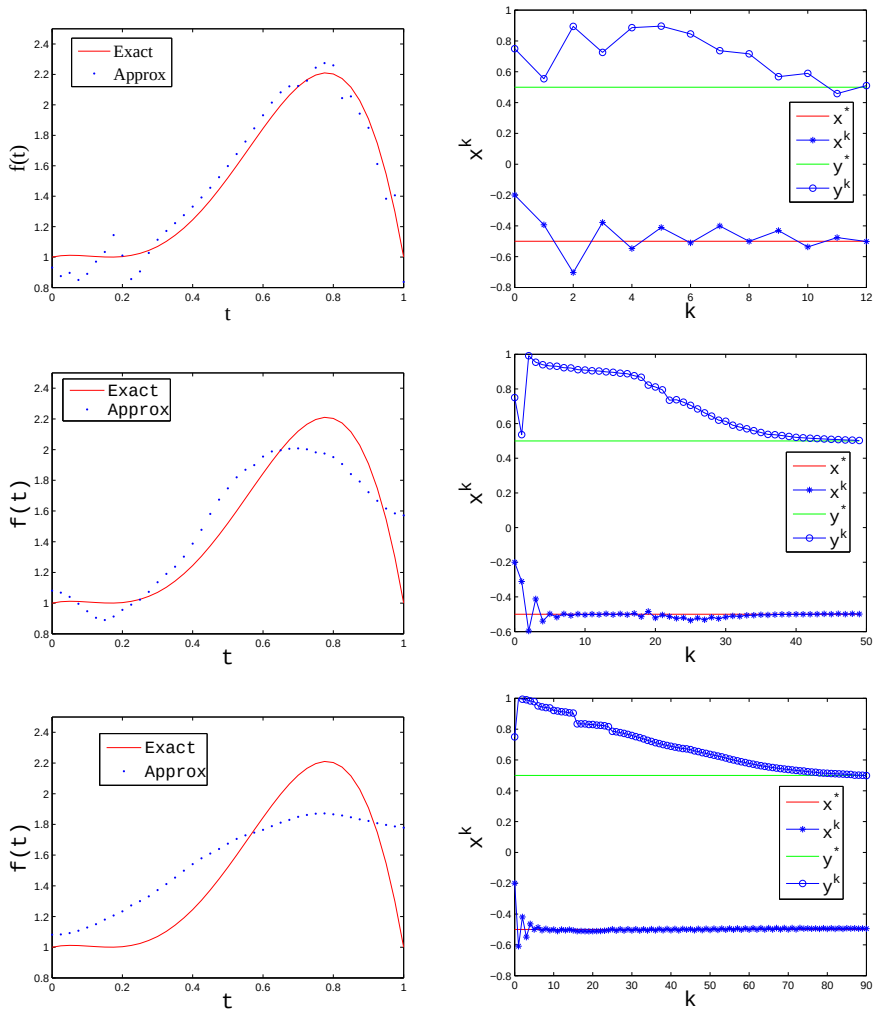

FIGURE 2. Reconstructions for Example 2 with different amount of measurement data with $N_s = 561$ (top), $N_s = 25$ (middle) and $N_s = 9$ (bottom).

Example 3. We take the true intensity function and the source location to be

$$f(t) = \begin{cases} 0.3\pi t\,, & 0 \le t < 0.5 \\ 0.15\pi\,, & 0.5 \le t < 0.7 \\ 0.5\pi - 0.5\pi t\,, & 0.7 \le t < 1.0 \end{cases}, \quad \mathbf{x}^* = (0.5, 0.75)$$

and the initial guess to the intensity to be $f^0(t) = t$. This example tests a piecewise smooth intensity function. We use a mesh 33×17 and time step size $\tau = 1/40$. Next we compare the performance of the averaging scheme and the scheme of approximated Dirac delta function proposed in section 4.4. To ensure the situations described therein to occur in our iterative process, i.e., some iterated approximation $\mathbf{x}^k$ of the source location lies at a mesh point or on some element edge, we consider the following two initial guesses for the source location:

(1) The initial guess lies on an element edge: $\mathbf{x}^0 = (0.88, 1.0)$.
(2) The initial guess is a mesh point: $\mathbf{x}^0 = (0.25, 0.25)$.

Note that in our settings the true source location $\mathbf{x}^*$ is also a grid point. Recall the three different approximated Dirac delta functions, namely $\delta_a^1, \delta_a^2, \delta_a^3$, for which we take the corresponding parameters to be $a = 0.01, 0.001, 0.001$ respectively. In this example we test the mixed BV and L^2 regularization, with the regularization parameters 5×10^{-8} and 2×10^{-6} respectively. See Figure 3-4 for the case with initial point $(0.88, 1.0)$ and Figure 5-6 for the case with initial point $(0.25, 0.25)$.

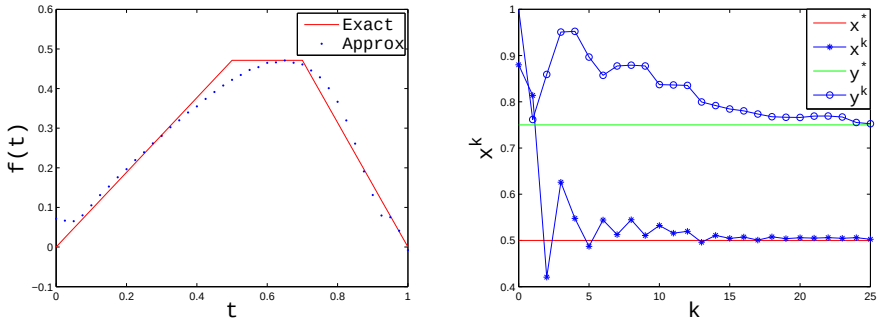

FIGURE 3. Reconstructions for Example 3 with initial guess $(0.88, 1.0)$ for the source location by the averaging scheme.

We observe from these figures that the schemes of using approximated Dirac delta function perform basically as well as the averaging scheme. So this verifies the effectiveness of our proposed treatments to obtain a reasonable approximate solution to the derivative equations (15) and (16).

Example 4. We take the exact intensity and the source location to be

$$f(t) = \begin{cases} 0.65, & 0 \le t < 0.5 \\ 0.3, & 0.5 \le t \le 1.0 \end{cases}, \quad \mathbf{x}^* = (-0.3, 0.1)$$

and their initial guesses to be

$$f^0(t) = t, \quad \mathbf{x}^0 = (-0.01, 0.3).$$

This example tests how our reconstruction algorithm works for recovering the discontinuous intensity, which is more challenging than the smooth cases. A natural regularization to handle discontinuity is the BV regularization. In this experiment we use the very coarse mesh 17×9 and the time step size $\tau = 1/40$, and apply the

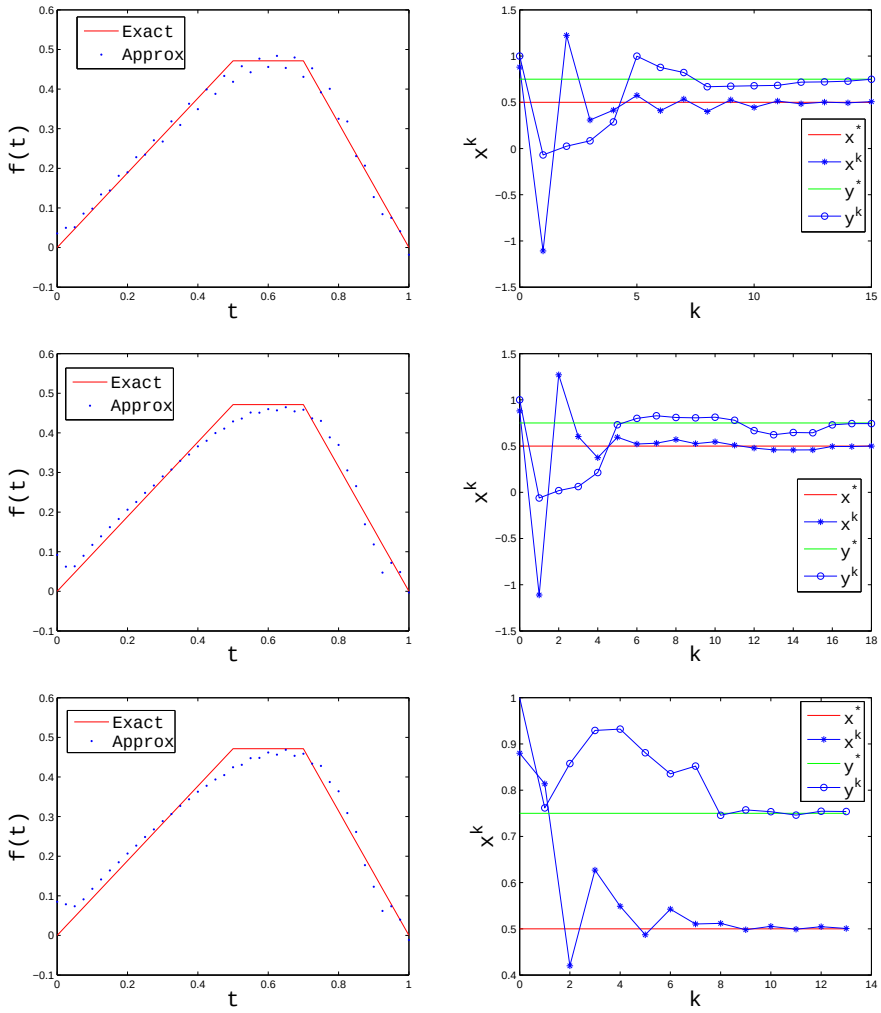

FIGURE 4. Reconstructions for Example 3 with initial guess $(0.88, 1.0)$ for the source location by the scheme of approximated Dirac delta function δ_a^1 (top), δ_a^2 (middle) and δ_a^3 (bottom).

approximated Dirac delta function approach proposed in section 4.4. We observe from Figure 7 that the numerical reconstruction is quite satisfactory.

6. Concluding remarks

This work investigates the numerical recovery of the source location and the corresponding time-dependent intensity using the measured data of concentration at the terminal time. The reconstruction is achieved by using the output least-squares formulation with appropriate regularizations, including L^2, H^1 and BV penalties. Our major focus is to have a detailed study of the space discretization of the resulting nonlinear optimization system by the piecewise linear finite element method, which is the least expensive finite element. For the reconstruction of the source location we need to evaluate the derivatives of linear finite element functions, but that are unfortunately not well-defined along all the common edges shared by two

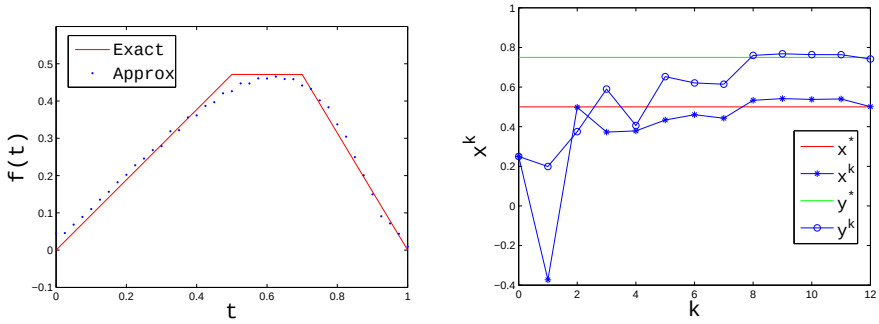

FIGURE 5. Reconstructions for Example 3 with initial guess $(0.25, 0.25)$ for the source location by the averaging scheme.

neighboring elements. Two effective numerical remedies, an averaging scheme and a scheme by the approximated Dirac delta functions, are proposed to overcome such difficulty. The numerical experiments have demonstrated the robustness and effectiveness of the reconstruction algorithms by the simplest and least expensive linear finite elements, in simultaneously recovering the source location and intensity, including both continuous and discontinuous cases. All the derivations and discussions of this work have been carried out for two space dimensions. But the algorithms and numerical remedies proposed here can be naturally extended to three space dimensions.

Acknowledgments

The work of Jun Zou was substantially supported by Hong Kong RGC grants (Projects 405110 and 404611) and a Direct Grant for Research from The Chinese University of Hong Kong.

References

[1] Atmadja, J. and Bagtzoglou, A.C., State of the art report on mathematical methods for groundwater pollution source identification, Environ. Forensics 2 (2001), 205-214.
[2] Balakrishnan, V., All about the dirac delta function (?), Resonance 8 (2003), 48-58.
[3] Jin, B. and Zou, J., Hierarchical Bayesian inference for ill-posed problems via variational method, J. Comput. Phys. 229 (2010), 7317-7343.
[4] Ciarlet, P.G., The Finite Element Method for Elliptic Problems, first ed., North-Holland Pub. Co., Amsterdam/New York, 1978.
[5] Engl,H.W., Hanke, M. and Neubauer, A., Regularization of Inverse Problems, Kluwer Academic Publishers, Netherland, 1998.
[6] Gorelick, S., Evans, B. and Remson, I., Identifying sources of groundwater pullution: an optimization approach, Water Resour. Res. 19 (1983), 779-790.
[7] Hamdi,A., The recovery of a time-dependent point source in a linear transport equation: application to surface water pollution, Inverse Problems 24 (2009), 1-18.
[8] Hamdi, A., Identification of a time-varying point source in a system of two coupled linear diffusion-advection- reaction equations: application to surface water pollution, Inverse Problems 25 (2009), 1-21.
[9] Ling, L., Yamamoto, M., Hon, Y. and Takeuchi, T., Identification of source locations in two-dimensional heat equations, Inverse Problems 22 (2006), 1289-1305.
[10] Khemka, A., Bouman, C. and Bell, M., Inverse problems in atmospheric dispersion with randomly scattered sensors, Digit. Signal Process 16 (2006), 638-651.
[11] Kathirgamanathan, P., McKibbin, R. and McLachlan, R.I., Source term estimation of pollution from an instantaneous point source, Res. Lett. Inf. Math. Sci. 3 (2002), 59-67.

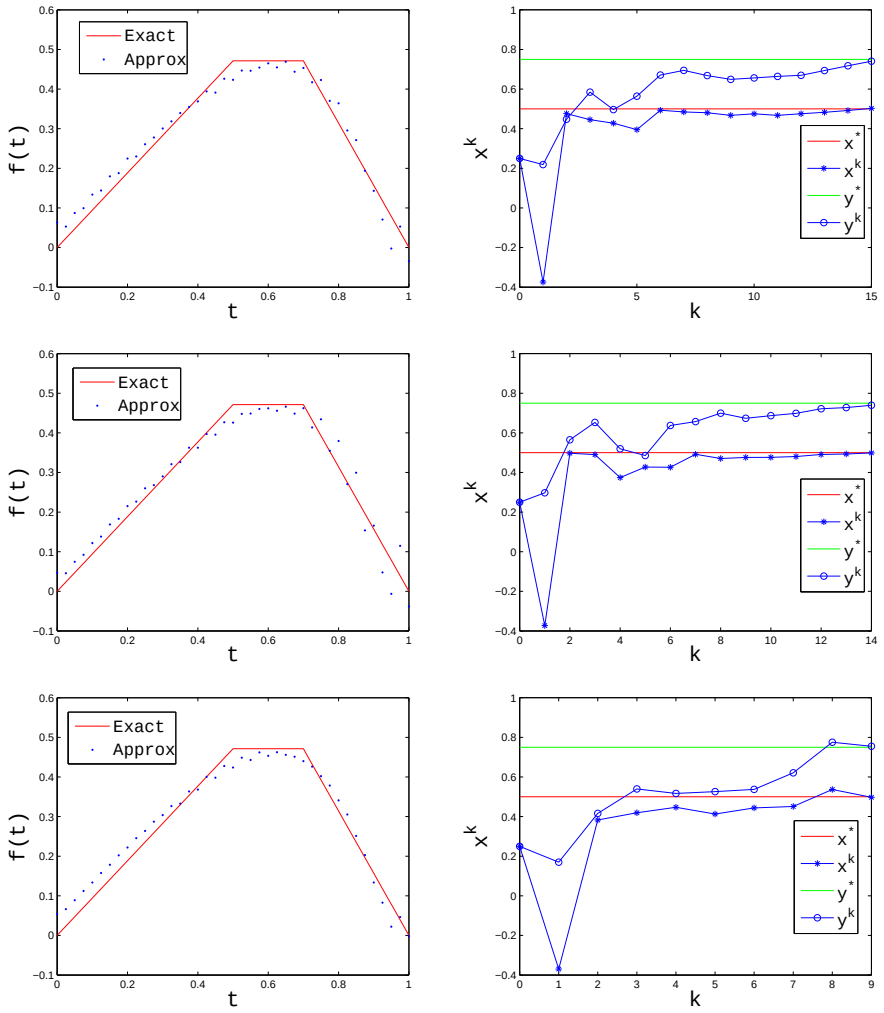

FIGURE 6. Reconstructions for Example 3 with initial guess $(0.25, 0.25)$ for the source location by the scheme of approximated Dirac delta function δ_a^1 (top), δ_a^2 (middle) and δ_a^3 (bottom).

[12] Kuhn, H.W. and Tucker, A.W., Nonlinear programming, Proceedings of 2nd Berkeley Symposium, Berkeley: University of California Press (1951), 481-492.
[13] Keung, Y.L. and Zou, J., Numerical identifications of parameters in parabolic systems, Inverse Problems 14 (1998), 83-100.
[14] Keung, Y.L. and Zou, J., An efficient linear solver for nonlinear parameter identification problems, SIAM. J. Sci. Comput. 22 (2000), 1511-1526.
[15] Revelli, R. and Ridolfi, L., Nonlinear convection-dispersion models with a localized pollutant source II–a class of inverse problems, Math. Comput. Model. 42 (2005), 601-612.
[16] T. Skaggs and Z. Kabala, Recovering the release history of a groundwater contaminant, Water Resour. Res. 30 (1994), 71-80.
[17] Skaggs, T. and Kabala, Z., Recovering the history of a groundwater contaminant plume: method of quasi-reversibility, Water Resour. Res. 31 (1995), 2669-2673.
[18] Samarskii, A.A. and Vabishchevich, P.N., Numerical Methods for Solving Inverse Problems of Mathematical Physics, Walter de Gruyter, Berlin, 2007.
[19] Woodbury, K.A., Inverse Engineering Handbook, CRC Press, 2003.

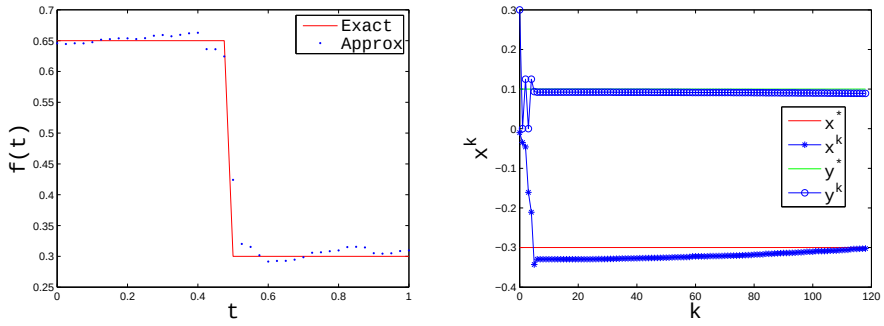

FIGURE 7. Reconstructions for Example 4 with discontinuous intensity function.

[20] Wong, J. and Yuan, P., A FE-based algorithm for the inverse natural convection problem, Int. J. Numer. Meth. Fluids 68 (2012), 48-82.
[21] Xie, J.L. and Zou, J., Numerical reconstruction of heat fluxes, SIAM J. Numer. Anal. 43 (2005), 1504-1535.

Laboratory for Engineering and Scientific Computing, Shenzhen Institutes of Advanced Technology, Chinese Academy of Sciences, Shenzhen, Guangdong 518055, China
E-mail: xm.deng@siat.ac.cn and yb.zhao@siat.ac.cn

Department of Mathematics, The Chinese University of Hong Kong, Shatin N.T., Hong Kong, P.R. China
E-mail: zou@math.cuhk.edu.hk